Kufa Journal of Engineering
Vol. 17, No. 2, April 2026, P.P. 387-400
Article history: Received 2 May 2025, last revised 1 July 2025, accepted 27 July 2025

ENHANCED BREAST TOMOSYNTHESIS RECONSTRUCTION USING DISTANCE-DRIVEN MAXIMUM LIKELIHOOD EXPECTATION MAXIMIZATION TECHNIQUE

Nuhad A. Malalla[1], Ali A. Al-azza[2], Suhad A. Malalla[3], Suroor M. Dawood[4], and Zaineb M. Alhakeem[5]

[1] Lecturer, PhD., Basrah University for Oil and Gas, College of Oil and Gas Engineering, Department of Chemical and Petroleum Refining Engineering, Basra, Iraq, Email:dr.nuhad@buog.edu.iq.

[2] Lecturer, PhD., University of Basrah, College of Engineering, Department of Electrical Engineering, Basra, Iraq, Email:ali.noaman@uobasrah.edu.iq.

[3] M.D. Iraqi Ministry of Health, Basra, Iraq, Email:suhadmalallah70@gmail.com.

[4] Lecturer, PhD., Basrah University for Oil and Gas, College of Oil and Gas Engineering, Department of Chemical and Petroleum Refining Engineering, Basra, Iraq, Email: suroor.moaid@buog.edu.iq.

[5] Assist. Professor, PhD., Basrah University for Oil and Gas, College of Oil and Gas Engineering, Department of Chemical and Petroleum Refining Engineering, Basra, Iraq, Email: zainebalhakeem@buog.edu.iq.

https://doi.org/10.30572/2018/KJE/170223

ABSTRACT

Early detection of breast cancer significantly improves patient outcomes through timely and accurate diagnosis. This study proposes a hybrid image reconstruction method combining the Maximum Likelihood Expectation Maximization (MLEM) algorithm with the Distance Driven Method (DDM) for stationary digital breast tomosynthesis, aimed at producing high-resolution three-dimensional (3D) breast images. The method was initially validated using simulated projection data of a digital breast phantom modeled with two spheres of varying radii and attenuation coefficients. Fifteen projection images were generated over a 15° angular range (from +7° to –7° with 1° increments) to replicate realistic tomosynthesis acquisition. The focus plane was set 45 mm above the detector with a pixel size of 0.14 mm. Reconstruction results demonstrated enhanced image quality, with spatial resolution quantitatively evaluated using the Line Spread Function (LSF) across the smaller sphere. Compared to the Ray Driven Method (RDM), the MLEM-DDM approach provided better contrast, sharper edges, and fewer artifacts.

Subsequently, the method was applied to experimental data from a real breast phantom. Volumetric reconstructions revealed detailed tissue structures across multiple planes, with spatial resolution assessed by line profiling through two aligned calcifications in the focus plane. The MLEM-DDM method preserved the shape and sharpness of these calcifications more effectively than MLEM-RDM. Overall, the proposed MLEM-DDM framework enhances spatial resolution and visualization quality in stationary digital breast tomosynthesis, demonstrating strong potential for improved early breast cancer detection and diagnostic accuracy.

KEYWORDS

Breast imaging, Tomosynthesis, Distance driven method (DDM), Maximum likelihood expectation maximization (MLEM).

1. INTRODUCTION

Detection of breast cancer at an early stage helps to increase the survival rate to 99% (American Cancer Society, 2019). Breast cancer is the second most common cancer among the women in the world. According to (Admoun & Mayrovitz, 2022), in United States approximately one of eight women in their lifetime have risk of development breast cancer. In Iraq, this tumor is the most common cancer among Iraqi women (Hashim et al., 2021). Statistics in Iraq shows an increase incidence of breast cancer between 2000 and 2009 from 26.6 per 100,000 to 31.5 per 100,000 ("Breast Cancer in Fallujah District (Iraq), A Comparative Pathological Study," 2020). For early breast cancer detection, one of American Cancer Sociality (ACS) recommendations is that the women after 45-years old should start to get mammogram imaging annually (American Cancer Society., 2020). There are many methods of breast cancer imaging each one has its own advantages and disadvantages such as Mammography, Digital Breast Tomosynthesis (DBT), Ultrasound, Magnetic Resonance Imaging (MRI), Contrast-Enhanced Mammography (CEM), Positron Emission Tomography (PET), and Breast Tomographic Ultrasound (BTUS). Among all these methods the mammography is the most common x-ray medical imaging technologies with low energy x-rays tubes (Coelho et al., 2023).

Mammography is usually used for breast examination to scan and diagnose either asymptomatic or symptomatic patients (Basurto-Hurtado et al., 2022; Ou et al., 2021). However, mammography provides two dimensional (2D) images for the breast tissues. The common problem of 2D images is the overlapping problem that makes the abnormal lump from over lying breast tissue difficult to distinguish especially for dense breast. Thus, the rate of false positive and false negative results increases. To overcome this problem, 3D mammography (Tomosynthesis) is developed (Chong et al., 2019; Shoshan et al., 2022) to provide 2D images along with 3D image for the compressed breast during the same exam and the same compression. Tomosynthesis is a limited angle tomography that an x-ray source fixed on arm that moves over the breast in a sight arc for acquiring multiple projection images for low total radiation exposure dosage (Asbeutah et al., 2020). To get volumetric information of the breast, reconstruction algorithms are used to work on the 2D projection data to reconstruct 3D planes of the breast tissues in way that enable radiologists to see through the breast.

2. THE LITRETURE REVIEW

Images in breast cancer could be processed according to different fields such as diagnosis from or classification, reconstruction , denoising and other types of processing. Theses processing types are applied to the medical image to ensure the clarity and enhance the diagnosis of breast cancer.

Deep Learning (DL) is used to classify images in general (Mohammed et al., 2022) and used in disease diagnosis (Hasan & Mazinani, 2025; Mansour et al., 2025)Some researchers are used DL in classifying the images of the cancer to healthy, non-health or according to the type of tumor cancer or benign. In (Abdulaal et al., 2024) used Convolution neural network (CNN) for image classification in both binary classes and multiclass with very promising performance. After that (Abdulaal et al., 2025), the authors used a hybrid model to classify the images using deep learning, the proposed hybrid neural network can reach over 99% of classification accuracy. In fact good classification need a clear image that leads to the image enhancement and bluer image reconstruction methods before the classification method is applied. The enhancement is needed to be applied instead of repeat the imaging process which will cost many and time.

In order to enhance the image quality with free motion artifacts, stationary tomosynthesis (Chen et al., 2009) is an alternative version technique of tomosynthesis that use a carbon nanotube x-ray source array that covering the field of view. The projection images are acquired by controlling the switching on/off of each individual tube electronically. Since stationary tomosynthesis is out of any mechanical motion so the scanning time is decreased, motion artifacts is reduced and the image quality is enhanced.

Maximum Likelihood Expectation Maximization (MLEM) is an iterative reconstruction algorithm for medical imaging techniques (Chuang et al., 2005). The imaging configurations can be modeled by linear equations, in the matrix form as AX=P where X is the image pixels vector, P is the projection values vector and A is the system matrix of the system coefficients. Each element in the system matrix represents the weight of contribution of each pixel to each projection ray.

In literatures, many studies (Chen et al., 2009; Zhou et al., 2010, 2015) used MLEM with Ray Driven Method (RDM) to compute the matrix of the system coefficient by calculating the segment length of the intersection between the projection ray and the pixel (ANDREW S. GLASSNER, 2019).

In addition to RDM, Distance Driven Method (DDM) was introduced in (Man & Basu, 2004) to calculate the matrix of the system which was applied on data from Computed Tomography (CT) technique. DM is used the convolution between the voxel (volumetric pixel) response and the detector response to find the overlap area between the voxel and the detector cell.

In this experiment, MLEM with DDM is used on stationary tomosynthesis technique to produce 3D tomosynthesis images. Firstly, MLEM with DDM is investigated on computer simulated projection images for simulation breast phantom to reconstruct 3D images. To mimic the breast,

two spheres with different radius and attenuation coefficient are simulated. The 15 projection images of the simulated phantom are acquired over view angle 15 degree. The reconstruction results show the details of the phantom. The spatial resolution is evaluated by line spread function that is used through the center of the smaller simulated sphere. Secondly, MLEM with DDM is applied on set of raw data for real breast phantom that were acquired from stationary breast tomosynthesis to reconstruct 3D tomosynthesis images of the breast. The volumetric results show the tissue structure of the phantom on different reconstruction planes. The line profile across the focus reconstruction plane through the center of two align calcifications shows the spatial resolution of the reconstruction plane. The shape and edges of tiny calcifications can be clearly identified.

This paper consists of four sections that are organized as follows:- in the first section, the introduction and the literature review of the previous studies are presented. In the second section, the methods and materials structure are described. The scenarios-results are demonstrated, analyzed, and validated in the third section. Finally, the study conclusions and future recommendations are elaborated in the last section.

3. METHODS AND MATERIALS

This section shows the methods and materials that are used in this work.

3.1. Imaging Configurations

The imaging configuration of stationary tomosynthesis is shown in Fig. 1. Raw data of compressed breast was collected from each x-ray tube by controlling the switching on/off of each x-ray tube. Projection images from different view angles are acquired over the total view angle Θ. Fig. 1 shows the 2D detector that is placed on (x-y) plane. The origin of 3D coordinate system (O) is located at the center of the detector plane where SID (Source to Image Distance) represents the distance between the x-ray sources to detector plane along z-axis and Source to Object Distance (SOD) is the perpendicular distance between x-ray tube and the center of the object (compressed breast).

3.2. Forward distance driven method (DDM)

To reconstruct three-dimensional (3D) object, the object is meshed into small voxels and each voxel is assigned an attenuation coefficient μ. The intensity of detected x-ray beam (Io) can be expressed by:

$$I_o = I_i e^{\sum_i w_{ij}\mu_j} \quad (1)$$

where Ii is the incident intensity of x-ray beam, μj is a linear attenuation coefficient of jth voxel and wij is the weight of the contribution of a given voxel to ith projection line.

The weight of the contribution of each voxel to each projection line is calculated by DDM by mapping boundaries of the voxels and detector cells into a reference axis to calculate the overlap length between the projected voxel and the projected detector cells. Fig. 2 shows two-dimensional forward distance driven method mapping. The given pixel and detector cells are projected to reference level. In this case, the detector plane of stationery tomosynthesis is parallel to the reference level. Consequently, the projection of detector cells participates with width of whole cells (P1, P2 and P3). The given pixel participates with value (O1, O2 and O3) which are the overlap length between the projected pixel and the projected detector cells.

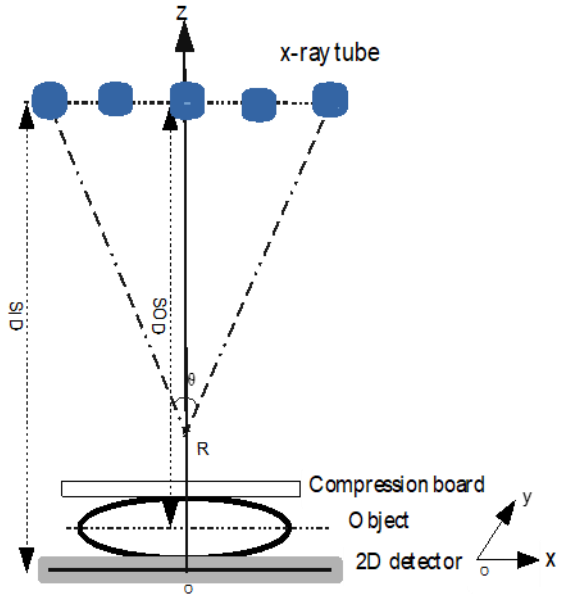

Fig. 1. Imaging configurations

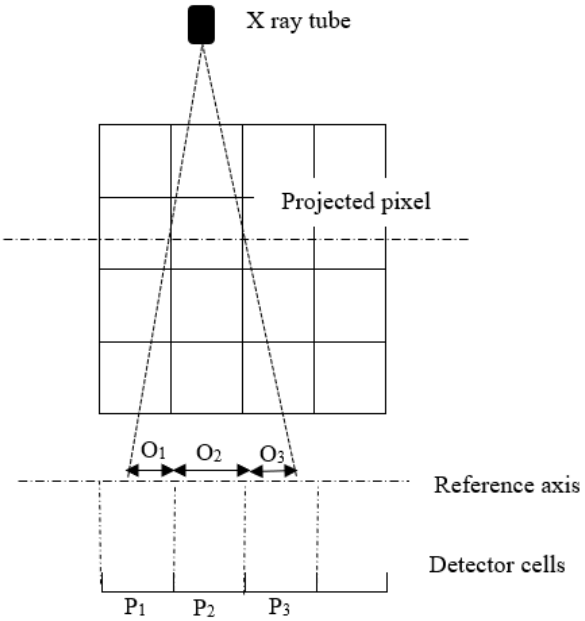

Fig. 2. Two-dimensional Forward distance driven method.

For 3D image voxels, the weights of DDM are computed by mapping both horizontal and

vertical boundaries of image voxels and detector cells onto a reference plane to calculate the area of the overlapping them.

3.3. Tomosynthesis Reconstruction Algorithms

After the projection process, raw data acquisition is obtained. The 2D projection images are sent to computer for processing with image reconstruction algorithm to create 3D images. Fully 3D evaluations need significant amount of data storage. This leads to an excessive demand for computing technologies in reconstruction. This paper focuses on using maximum likelihood expectation maximization (MLEM) technique as a solution for the above issue as shown in Fig.3.

MLEM is a statistical reconstruction algorithm which is under an assumption that the incident and transmitted x-ray intensities follow Poisson statistics. The linear attenuation coefficient μ of j^{th} voxel is updated by:

$$\mu_j^{(t+1)} = \mu_j^t + \frac{\mu_j^t \sum_i w_{ij} \left(I_i e^{-\sum_i w_{ij}\mu_j^t} - O_i\right)}{\sum_i (w_{ij} \langle w, \mu^t \rangle I_i \, e^{-\sum_i w_{ij}\mu_j^t})} \qquad (2)$$

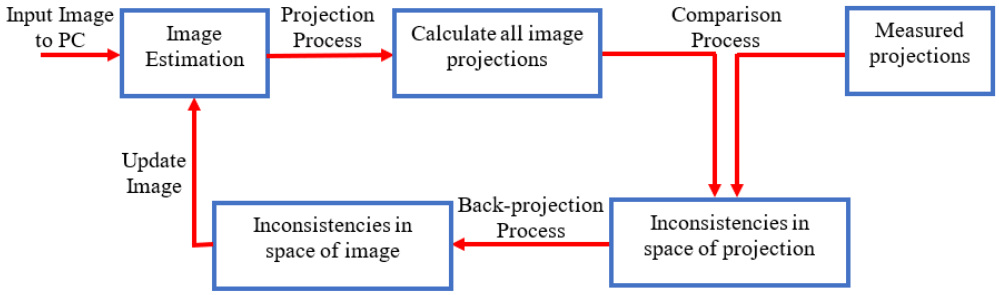

Fig. 3. The MLEM basic procedures diagram

Where: O_i is the detected x-ray intensity and I_i is the incident intensity of of i^{th} pixel. w_{ij} is the weight of contribution of i^{th} ray for j^{th} voxel. The DDM-MLEM technique flow chart is given in Fig. 4:

Where in Fig. 4 above P: Measured projection dataset (acquired by tomosynthesis)

A_p: Projection system operator (according to DDM)

N_{it}: Iterations number used

f_{im}: initial estimated-image

S_{map}: Precomputed sensitivity-map

P_f: Forward estimated projection

C_M: Correction Matrix

f_{new}: *Updated 3D Image*

ε: Small constant value to avoid division by zero.

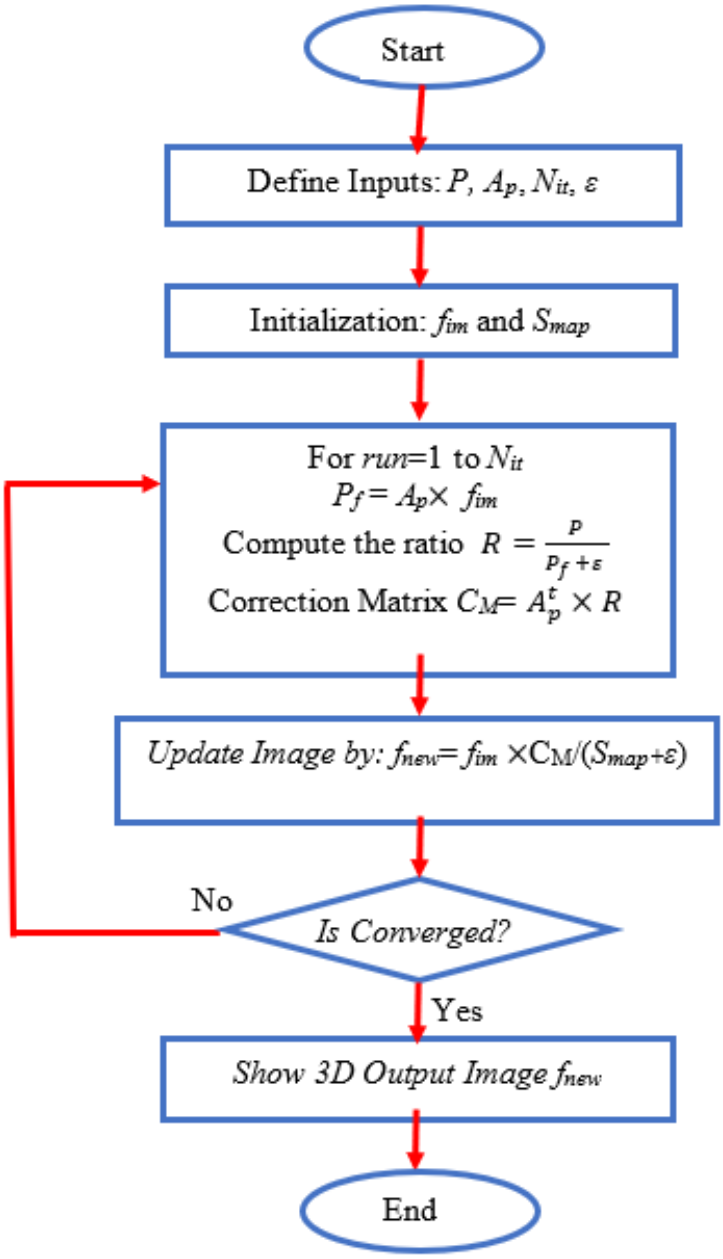

Fig. 4. The DDM-MLEM algorithm flow chart

4. RESULTS

To imitate a breast with a mass, two spherical objects were simulated with different sizes respectively. The mass was simulated as solid sphere with the attenuation coefficient of 0.038 mm-1. In the present work, the values of SID and SOD are 692.8 mm and 650 mm, respectively. Simulated raw data was collected from over view angle equals to 15o with step size 1o. Table1 lists the coordinates of source location at each projection angle. The focus plane across the center of the simulated mass is placed at 45 mm from the detector plane. Additionally, the system detector is simulated with pixel size of 0.14mm.

Table 1 The locations of X-ray source.

θ	x	y	z
-7^o	4.48	−79.80	692.8
-6^o	4.48	−68.31	692.8
-5^o	4.48	−56.86	692.8
-4^o	4.48	−45.45	692.8
-3^o	4.48	−34.06	692.8
-2^o	4.48	−22.69	692.8
-1^o	4.48	−11.34	692.8
0^o	4.48	0.00	692.8
1^o	4.48	11.34	692.8
2^o	4.48	22.69	692.8
3^o	4.48	34.06	692.8
4^o	4.48	45.45	692.8
5^o	4.48	56.86	692.8
6^o	4.48	68.31	692.8
7^o	4.48	79.80	692.8

The 15 projection images are collected from the x-ray sources through projection angles of 7^o to -7^o with 1^o step angle. Fig.5 presents three projection images at angle 7^o, 0^o, -7^o.

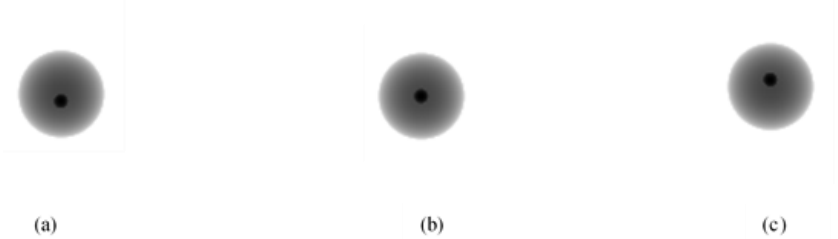

Fig. 5. Projection images at angles: a. 7^o b. 0^o c. -7^0.

MELM with DDM and MELM with RDM `are applied on acquired projection data to reconstruct 3D images. The reconstructed focus plane through the center of simulated mass at height at 45 mm of both methods are shown in Fig.6.

a **b**

Fig. 6. The reconstructed focus plane of simulated mass by: (a) MELM with DDM (b) MELM with RDM

To demonstrate the spatial resolution, the line spread function across the center of the simulated mass of focus planes of both methods are shown in Fig. 7. The line profile of DDM shows better contrast, sharper edges and less artifacts.

This experiment was also done on real breast phantom with circular mass with six tiny calcifications with size of micrometer. 15 projection images were acquired over 15^o view angle with 1^o angular step size. The projection images at angle 0^o shows in Fig. 8.

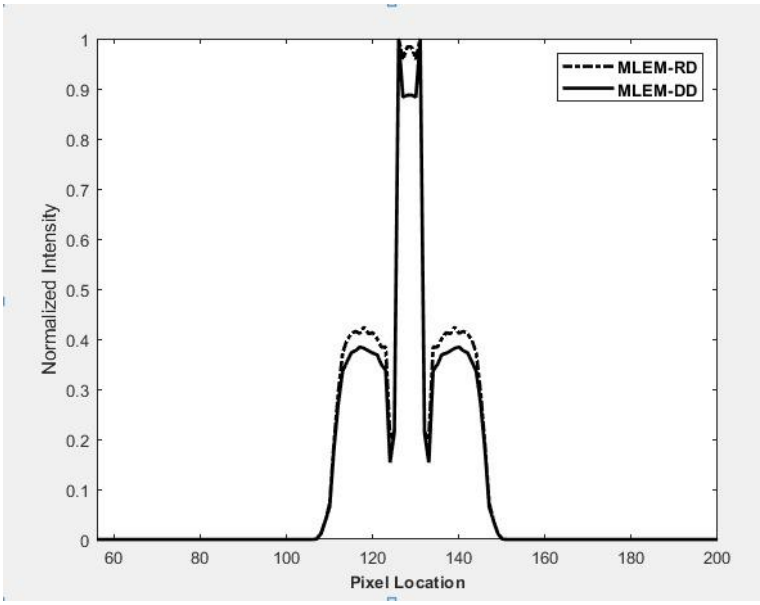

Fig. 7. Line profile across the center of simulated mass.

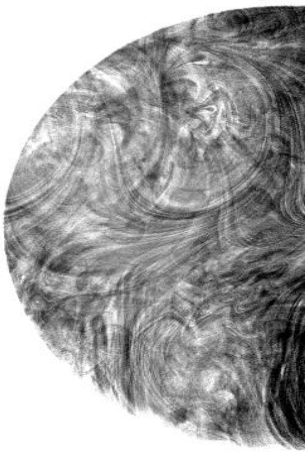

Fig.8. Projection view of breast phantom at angle 0º

Fig. 9 shows the reconstructed focus plane and the region of interest (ROI) of reconstructed focus plane of breast phantom.

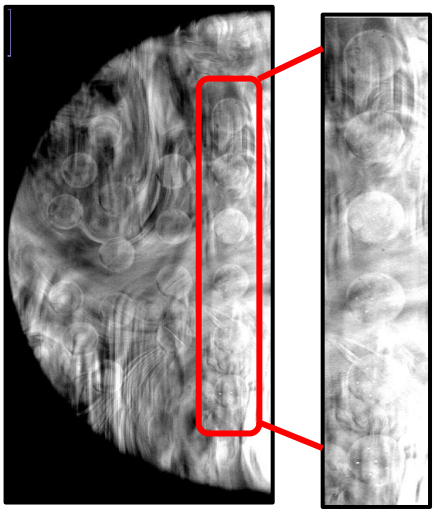

Fig 9. Focus plane of real phantom and its ROI of circilur mass.

The line profile across the focus reconstruction plane through the center of two align calcifications shows the spatial resolution of the reconstruction plane. The shape and edges of tiny calcifications can be clearly identified as shown in Fig 10.

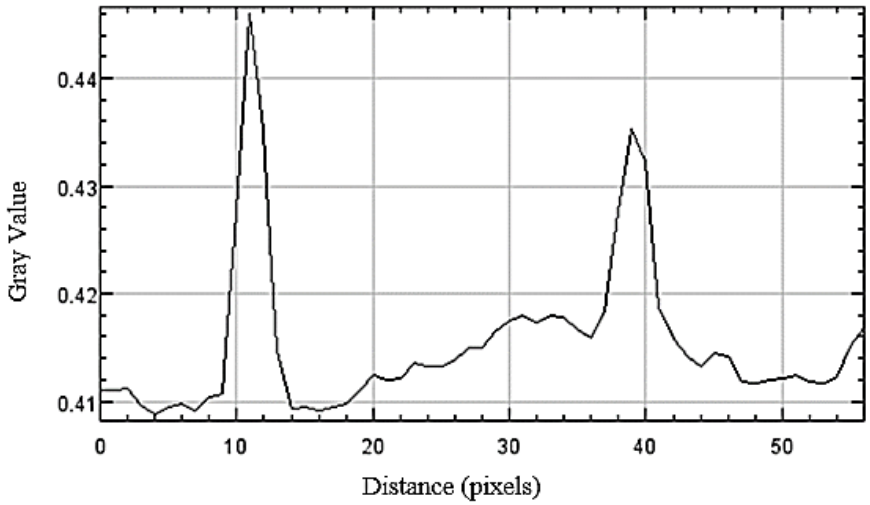

Fig. 10. Line profile across the two tiny calcifications.

5. CONCLUSIONS

This study demonstrates that the integration of the Maximum Likelihood Expectation Maximization (MLEM) algorithm with the Distance Driven Method (DDM) significantly enhances the reconstruction of high-resolution three-dimensional breast images in stationary digital breast tomosynthesis. Initial validation on simulated breast phantom data—featuring spheres with varying sizes and attenuation coefficients—confirmed that the MLEM-DDM approach delivers superior image quality, characterized by better contrast, sharper edges, and fewer artifacts than the conventional Ray Driven Method (RDM). Spatial resolution was quantitatively verified through the Line Spread Function (LSF), applied across the smaller sphere in simulation and through two aligned calcifications in experimental data.

Application to real breast phantom data further substantiated these findings, revealing clear tissue structures across multiple reconstruction planes. The reconstructed focus plane distinctly displayed a circular mass containing six tiny calcifications, with the shape and edges of two aligned calcifications particularly well-preserved. These improvements in spatial resolution and detail preservation are critical for enhancing the accuracy and confidence in early breast cancer detection.

Looking forward, combining stationary tomosynthesis with complementary imaging modalities such as MRI or ultrasound could provide more comprehensive diagnostic insights. Advancements such as adaptive DDM kernels may further refine reconstruction accuracy. Additionally, integrating MLEM-DDM outputs with machine learning and deep learning

algorithms holds promise for automated detection and classification, potentially broadening the applicability of this approach to other medical imaging fields and improving early diagnostic workflows.

6. REFERENCES

Abdulaal, A. H., Valizadeh, M., Yassin, R. A., Amirani, M. C., Shah, A. F. M. S., Albaker, B. M., & Mustaf, A. S. M. (2025). Hybrid CNN and RNN Model for Histopathological Sub-Image Classification in Breast Cancer Analysis Using Self-Learning. Journal of Engineering and Sustainable Development, 29(3), 310–320. https://doi.org/10.31272/jeasd.2746

Abdulaal, A. H., Yassin, R. A., Valizadeh, M., Abdulwahhab, A. H., Jasim, A. M., Mohammed, A. J., Jabir, H. J., Albaker, B. M., Dheyaa, N. H., & Amirani, M. C. (2024). CUTTING-EDGE CNN APPROACHES FOR BREAST HISTOPATHOLOGICAL CLASSIFICATION: THE IMPACT OF SPATIAL ATTENTION MECHANISMS. ShodhAI: Journal of Artificial Intelligence, 1(1). https://doi.org/10.29121/shodhai.v1.i1.2024.14

Admoun, C., & Mayrovitz, H. N. (2022). The Etiology of Breast Cancer. In Breast Cancer (pp. 21–30). Exon Publications. https://doi.org/10.36255/exon-publications-breast-cancer-etiology

American Cancer Society. (2019). Breast cancer facts & figures 2019–2020.

American Cancer Society. (2020). ACS Breast Cancer Early Detection Recommendations.

ANDREW S. GLASSNER. (2019). An introduction to ray tracing (13th ed.). ACADEMIC PRESS.

Asbeutah, A. M., AlMajran, A. A., Brindhaban, A., & Asbeutah, S. A. (2020). Comparison of radiation doses between diagnostic full-field digital mammography (FFDM) and digital breast tomosynthesis (DBT): a clinical study. Journal of Medical Radiation Sciences, 67(3), 185–192. https://doi.org/10.1002/jmrs.405

Basurto-Hurtado, J. A., Cruz-Albarran, I. A., Toledano-Ayala, M., Ibarra-Manzano, M. A., Morales-Hernandez, L. A., & Perez-Ramirez, C. A. (2022). Diagnostic Strategies for Breast Cancer Detection: From Image Generation to Classification Strategies Using Artificial Intelligence Algorithms. Cancers, 14(14), 3442. https://doi.org/10.3390/cancers14143442

Breast Cancer in Fallujah District (Iraq), A Comparative Pathological Study. (2020). Medico-Legal Update. https://doi.org/10.37506/mlu.v20i2.1157

Chen, Y., Zhou, W., Yang, G., Qian, X., Lu, J., & Zhou, O. (2009). Breast tomosynthesis reconstruction with a multi-beam x-ray source (E. Samei & J. Hsieh, Eds.; p. 725859). https://doi.org/10.1117/12.811659

Chong, A., Weinstein, S. P., McDonald, E. S., & Conant, E. F. (2019). Digital Breast Tomosynthesis: Concepts and Clinical Practice. Radiology, 292(1), 1–14. https://doi.org/10.1148/radiol.2019180760

Chuang, K.-S., Jan, M.-L., Wu, J., Lu, J.-C., Chen, S., Hsu, C.-H., & Fu, Y.-K. (2005). A maximum likelihood expectation maximization algorithm with thresholding. Computerized Medical Imaging and Graphics, 29(7), 571–578. https://doi.org/10.1016/j.compmedimag.2005.04.003

Coelho, F. M. de O., Gontijo, M. F. S. V., Loaiza, K. P. C., Franco, R. C. S., & Avelar, J. T. C. de. (2023). Advances in breast imaging: a review on where we are and where we are going. Mastology, 33. https://doi.org/10.29289/2594539420230001

Hasan, A., & Mazinani, M. (2025). DETECTION OF KERATOCONUS DISEASE DEPENDING ON CORNEAL TOPOGRAPHY USING DEEP LEARNING. Kufa Journal of Engineering, 16(1), 463–478. https://doi.org/10.30572/2018/KJE/160125

Hashim, H. T., Ramadhan, M. A., Theban, K. M., Bchara, J., El-Abed-El-Rassoul, A., & Shah, J. (2021). Assessment of breast cancer risk among Iraqi women in 2019. BMC Women's Health, 21(1), 412. https://doi.org/10.1186/s12905-021-01557-1

Man, B. De, & Basu, S. (2004). Distance-driven projection and backprojection in three dimensions. Physics in Medicine and Biology, 49(11), 2463–2475. https://doi.org/10.1088/0031-9155/49/11/024

Mansour, H. S., Valizadeh, M., Abdulaal, A. H., & Amirani, M. C. (2025). A Novel Deep 2D-CNN Model for ECG-Based Arrhythmia Diagnosis with Selective Attention Mechanism and CWT Integration. Kufa Journal of Engineering, 16(2), 423–444. https://doi.org/10.30572/2018/KJE/160225

Mohammed, H. A., Kareem, S. W., & Mohammed, A. S. (2022). A COMPARATIVE EVALUATION OF DEEP LEARNING METHODS IN DIGITAL IMAGE CLASSIFICATION. Kufa Journal of Engineering, 13(4), 53–69. https://doi.org/10.30572/2018/KJE/130405

Ou, X., Chen, X., Xu, X., Xie, L., Chen, X., Hong, Z., Bai, H., Liu, X., Chen, Q., Li, L., & Yang, H. (2021). Recent Development in X-Ray Imaging Technology: Future and Challenges. Research, 2021. https://doi.org/10.34133/2021/9892152

Shoshan, Y., Bakalo, R., Gilboa-Solomon, F., Ratner, V., Barkan, E., Ozery-Flato, M., Amit, M., Khapun, D., Ambinder, E. B., Oluyemi, E. T., Panigrahi, B., DiCarlo, P. A., Rosen-Zvi, M., & Mullen, L. A. (2022). Artificial Intelligence for Reducing Workload in Breast Cancer Screening with Digital Breast Tomosynthesis. Radiology, 303(1), 69–77. https://doi.org/10.1148/radiol.211105

Zhou, W., Lu, J., Zhou, O., & Chen, Y. (2015). Ray-tracing-based reconstruction algorithms for digital breast tomosynthesis. Journal of Electronic Imaging, 24(2), 023028. https://doi.org/10.1117/1.JEI.24.2.023028

Zhou, W., Qian, X., Lu, J., Zhou, O., & Chen, Y. (2010). Multi-beam x-ray source breast tomosynthesis reconstruction with different algorithms. 76220H. https://doi.org/10.1117/12.844295